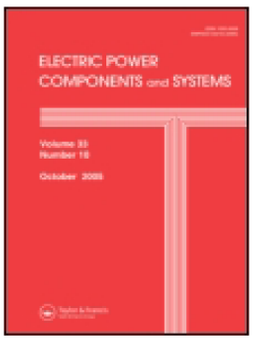

Taylor & Francis
Taylor & Francis Group

Electric Power Components and Systems

ISSN: 1532-5008 (Print) 1532-5016 (Online) Journal homepage: http://www.tandfonline.com/loi/uemp20

Maximum Lifecycle Tracking for Tidal Energy Generation System

Taofeek Orekan, Zhibing Zhao, Peng Zhang, Jian Zhang, Shengli Zhou & Jun-Hong Cui

To cite this article: Taofeek Orekan, Zhibing Zhao, Peng Zhang, Jian Zhang, Shengli Zhou & Jun-Hong Cui (2015) Maximum Lifecycle Tracking for Tidal Energy Generation System, Electric Power Components and Systems, 43:8-10, 1182-1192, DOI: 10.1080/15325008.2015.1010664

To link to this article: https://doi.org/10.1080/15325008.2015.1010664

Published online: 11 May 2015.

Submit your article to this journal

Article views: 942

View related articles

View Crossmark data

Full Terms & Conditions of access and use can be found at
http://www.tandfonline.com/action/journalInformation?journalCode=uemp20

Download by: [University of Connecticut] **Date:** 11 January 2018, At: 13:38

Electric Power Components and Systems, 43(8–10):1182–1192, 2015
Copyright © Taylor & Francis Group, LLC
ISSN: 1532-5008 print / 1532-5016 online
DOI: 10.1080/15325008.2015.1010664

Taylor & Francis
Taylor & Francis Group

Maximum Lifecycle Tracking for Tidal Energy Generation System

Taofeek Orekan,[1] Zhibing Zhao,[1] Peng Zhang,[1] Jian Zhang,[1] Shengli Zhou,[1] and Jun-Hong Cui[2]
[1]Department of Electrical and Computer Engineering, University of Connecticut, Connecticut, Storrs, USA
[2]Department of Computer Science and Engineering, University of Connecticut, Connecticut, Storrs, USA

Downloaded by [University of Connecticut] at 13:38 11 January 2018

CONTENTS

Abstract— The tidal energy conversion system has become a major facility for ocean energy harvesting. The intermittency of tidal currents and the resulting large cyclic stresses in the tidal generator, however, make the energy harvesting from tidal currents more challenging than from other renewable sources, such as wind and solar. This paper presents a concept of maximum life-cycle tracking, which minimizes, the torque stress on the shaft, therefore maximizing the life cycle of the tidal energy systems by tracking power-speed curves with a power electronic inverter. By implementing the new concept, the life cycle of a the tidal generator can be extended tens of times.

1. INTRODUCTION

The world's interest in the development of renewable source of energy from the ocean has increased rapidly in the past decades. The ocean possesses an enormous amount of clean renewable energy. Among the various ocean energy technologies under development, tidal turbines are gaining increasing attention because of their efficiency and scalability. The tidal power system was one of the first ocean energy technologies to be commercialized. In the 1960s, a large-scale barrage was built in La Rance, France and small-scale tidal turbines, have also been prototyped for research purposes[1, 2].

The kinetic energy from the moving water drives a tidal turbine, which is then converted from the mechanical energy to electrical energy by a generator, then transfering the electricity produced to an onshore power station through underwater power cables [3]. In most cases, power electronics are required to condition the power output before interconnection with the grid. The reliability of power electronic devices in a renewable energy generation system was discussed in [4]. The majority of the tidal energy converters use a permanent magnet synchronous generator (PMSG) because it shows a very high robustness compared to other types of generators, and it is driven directly by the turbine hub [5]. The harsh behavior of the ocean environment in which the tidal turbines are installed

Keywords:: Maximum lifecycle tracking, power electronic converters, tidal power generation, torsional stress, ocean energy, neural network
Received 3 December 2014; accepted 6 January 2015
Address correspondence to Prof. Peng Zhang, Department of Electrical and Computer Engineering, University of Connecticut, 371 Fairfield Way, Unit 2155, Storrs, CT 06269. E-mail: peng@engr.uconn.edu
Color versions of one or more of the figures in the article can be found online at www.tandfonline.com/uemp.

Downloaded by [University of Connecticut] at 13:38 11 January 2018

and operated leads to severe risks and high costs. They are often exposed to alternating loads in the bottom of the ocean, which is 800 times denser than air. These conditions affect the operations of the tidal energy drive train and the life cycle of critical components, such as the tidal turbine shaft. The power take-off train of a tidal turbine consisting of a shaft is a highly stressed subsystem that works continuously in terms of operational time. At a rotating speed of one-third of the speed of the wind turbine under the same power ratings, the tidal turbine shaft absorbed larger cyclic stress. With high cycle fatigue, the number of cycles and their amplitudes lead to failure in a short period, thereby affecting the performance of the generator and the production of electricity.

In 2009, an incident occurred in the Bay of Fundy on the Atlantic coast of North America, which resulted in failure of a 1 MW tidal turbine generator shaft, shown in Figure 1, after 20 days of installation. The failure was attributed to the high tidal current speed, caused torsional shaft oscillations and destroyed the turbine rotor blades [6]. Shaft fatigue in tidal generation following severe disturbances was investigated in [7–10]. While it is easy for an underwater system to fail under the extreme conditions, it is also difficult to maintain and repair. Therefore, reliability becomes a critical consideration during design and operation of a tidal turbine-generator system. A reliability model with a variable failure rate was developed in [11]. The authors used Monte Carlo simulation to generate the failure rate distribution, and a 90% confidence interval was determined. However, little work has been published on life-cycle extension of a tidal energy generation system.

This article uses an innovative control strategy called maximum life cycle tracking (MLCT) to address shaft failure problems in a tidal energy generation. As a timely contribution to the emerging field of tidal power technology, MLCT combines maximum power point tracking (MPPT) and the constant torque control strategy to extend the life cycle of tidal turbines. MPPT is a popular adaptive control strategy that extracts the maximum available power in a conversion system. It has been used successfully in renewable energy technologies, especially in photovoltaic and wind power generation [12, 13]. In a tidal generation system, the reference of the rotational speed control loop is adjusted such that the turbine operates around the maximum power of the tidal speed. However, when the tidal speed exceeds 2.5 m/s and becomes high, the mechanical torque becomes high as well, adding to the stress on the turbine. To mitigate the stress, the MLCT methodology applies a constant torque strategy to the tidal turbine at a high tidal speed range. Detailed case studies are presented based on a real-time digital simulator model of a tidal turbine that employs a PMSG and connects to the grid through a back-to-back converter interface. The rest of this article is organized as follows. In Section 2, the torques and fatigue are analyzed. In Section 3, the MLCT control strategy is described and compared with MPPT. In Section 4, the MLCT control and simulation results are presented. The conclusion is given in Section 5.

FIGURE 1. A 10-tonne tidal turbine destroyed at the Bay of Fundy, Nova Scotia. ©[CBC News]. Reproduced by permission of CBC News. Permission to reuse must be obtained from the rightsholder.

2. DRIVE TRAIN MODELING AND FATIGUE ANALYSIS

The system configuration under study is shown in Figure 2, where the PMSG is driven by a tidal turbine. Details of the system model can be found in Appendix A. In the turbine-generator system, the mechanical torque is applied to the turbine blades, and the electromagnetic torque is applied to the generator in the opposite direction. The mechanical dynamic equation of a generator is given by

$$J\frac{d\omega}{dt} + D\omega = T_m - T_e, \tag{1}$$

where T_m is the mechanical torque, T_e is the electromagnetic torque, D is the friction, and J is the joint moment of inertia of the turbine and generator. The single mass equation is adopted because the drive train and generator rotates as a whole, and the shaft is quite rigid for modern tidal systems. Moreover, the friction can also be omitted in the analysis without affecting the final results.

The interaction of both mechanical torque and electromagnetic torque causes stress on the turbine blades and shaft,

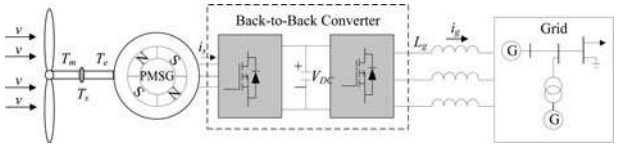

FIGURE 2. Tidal system configuration.

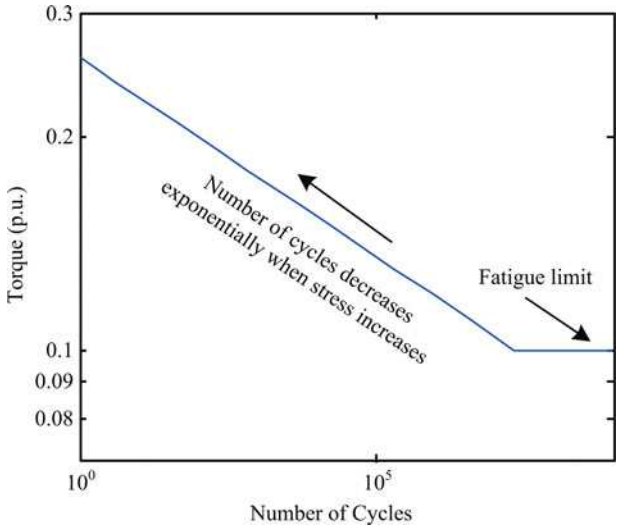

FIGURE 3. Torque-life curve.

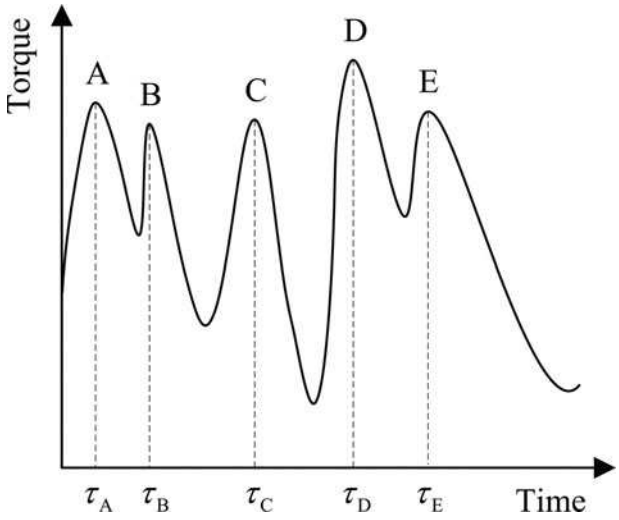

FIGURE 4. Torque-time curve.

leading to fatigue, which eventually results in failure. The relation between torque and the life cycle of the shaft is described through a torque-life curve in Figure 3. The number of cycles can be calculated using the following equation:

$$N = \frac{1}{2}\left(6.4 \times 10^{-6}\frac{\tau}{R_0^3}\right)^{-17.86}, \tag{2}$$

where N is the number of cycles the shaft can endure, R_0 is the radius of the shaft, and τ is the maximum torque in each cycle. The value $\left(6.4 \times 10^{-6}\right)$ is different for every shaft, and it is calculated based on the properties of the shaft material. Equation (2) is used to esimate the life cycle of the shaft under the assumption that the material is the same as that in [8]. Above the fatigue limit in Figure 3, the number of cycles decreases exponentially with stress, indicating the effect of stress on the tidal turbine shaft. However, in actual application, the shaft undergoes complex stress variations; therefore, the maximum torque is not constant in each cycle. To calculate fatigue damage under these conditions, a standard technique called Miner's rule is used, which can be expressed mathematically as

$$D_{life} = \Sigma\frac{n_i}{N_{fi}}, \tag{3}$$

where n_i number of cycles at the ith torque, N_{fi} is the number of cycles to failure at the ith torque, and D_{life} is the fraction of life expended.

When the fraction of life expended equals one, the Miner's rule predicts failure of the shaft. The number of cycles and the magnitude of each cycle are determined by the rainflow counting method [14]. Figure 4 shows a typical torque-time curve, which may occur for a given shaft. Each identifiable positive torque peak (labeled A, B, C, D, E) is counted as one cycle of a torque equal to the value of that peak. The rotation of Figure 4 by 90% forms Figure 5, which shows the half-circles and its magnitude. In this figure, the raindrop goes from starting point S through P_1 and ends at the V_2 dashed line because V_2 is lower than the S. The same mechanism works for the raindrops from V_1, V_2, V_3, etc. The raindrop from peak P_1 goes through V_1, V_2, and V_3 and ends at the P_4 dashed line

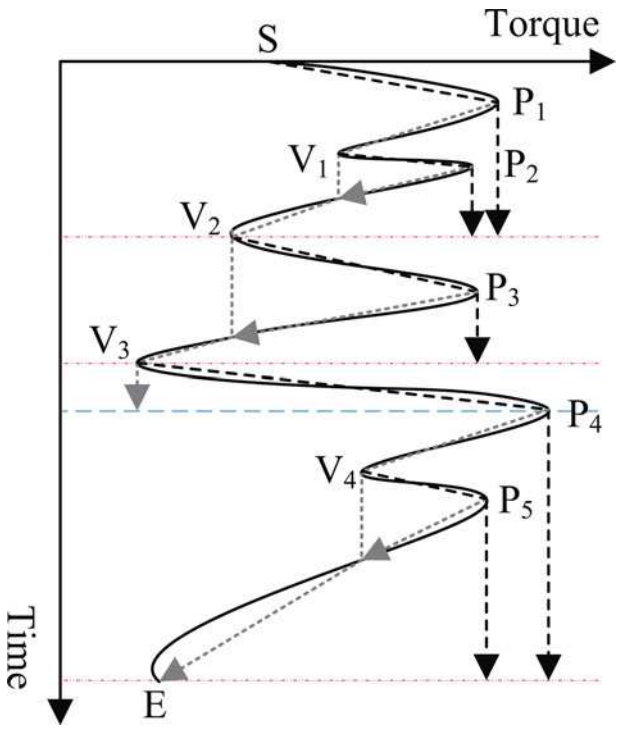

FIGURE 5. Rainflow counting method.

Downloaded by [University of Connecticut] at 13:38 11 January 2018

Downloaded by [University of Connecticut] at 13:38 11 January 2018

because P_4 is higher than the starting peak P_1. The raindrops from P_2, P_3, and P_5 stop at the paths of a previous raindrop. Hence, the difference between the starting point and the ending point is twice the magnitude of that half-cycle. Note that this is only a statistical estimation caused by stress. In reality, other factors, such as corrosion, which is out of the scope of this article, could also result in a shorter life.

To analyze the torque on the shaft, the torque at cross-section s in the shaft is considered, which is T_s. The mechanical equations are

$$J_T \frac{d\omega}{dt} = T_m - T_s, \tag{4}$$

$$J_G \frac{d\omega}{dt} = T_s - T_e, \tag{5}$$

where J_T is the moment of inertia of the tidal turbine, and J_G is moment of inertia of the generator. The total inertia on the shaft is therefore given by

$$J_T + J_G = J, \tag{6}$$

Substituting Eq. (4) into Eq. (5), gives

$$T_s = \frac{J_T T_e + J_G T_m}{J}. \tag{7}$$

The moment of inertial of tidal generator J_G is generally 10^{-3}kg m^2, which is quite small compared to the moment of inertial of a tidal turbine, which could reach a value as high as 10^4 kg $\cdot$ m^2 [15]. Thus, the torque on shaft T_s is mainly determined by electromagnetic torque T_e.

3. CONTROL STRATEGY

The present control strategy for tidal generation system incorporates MPPT, which adjusts the rotor speed to maximize the turbine output power, and a new (MLCT) strategy. The power harnessed by a tidal turbine can be calculated by the following equation:

$$P = \frac{1}{2}\rho C_P \pi R^2 V^3 \tag{8}$$

Here C_P is known as the turbine power coefficient, which depends on the turbine blade design and its hydrodynamics. Typically, the optimal C_P value of a tidal turbine for normal operation is in the range of 0.35–0.5 [16]. Figure 6 illustrates the tidal turbine characteristics at different tidal speeds, and the extractable power is calculated based on Eq. (8). In this figure, the black dashed line is the conventional MPPT control strategy curve. The mechanical torque T_m is the slope of the straight line connecting the operating point to the origin. It rises fast as the operating point goes up along the maximum power point (MPP) line. Therefore, when the tidal current speed is very high, e.g., 3 m/s, mechanical torque T_m increases as well. At the steady state, the electromagnetic torque is equal to the mechanical torque and adds to the stress on the shaft and turbine blades.

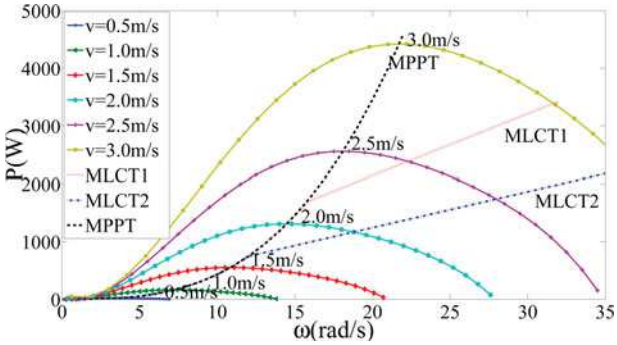

FIGURE 6. Turbine characteristics and control strategies

To mitigate the stress, an MLCT strategy is introduced, as shown in Figure 6. It is a combination of the MPPT control strategy and the constant torque control strategy. At low tidal current speeds, for instance 1 m/s, the MLCT strategy tracks the MPPs. As the tidal current speed increases to a specified point, it switches and tracks the red or blue line for which its extension in the opposite direction passes the origin. Figure 6 gives two examples of MLCT strategies. MLCT control 1 extracts more power than control 2; however, control 2 applies lower torque on the tidal shaft and blades. Hence, the choice of controller depends on the strength of the shaft.

3.1. Tidal Speed Estimation and Reference Generation

Traditionally, the measurement of tidal current speed using a flow-meter or other type of sensor is necessary for the controllers to generate the reference rotating speed of the turbine. However, these sensors are expensive to install and maintain underwater. Thus, artificial neural network (ANN) is used that is supplied with captured power and rotating speed to estimate the tidal current speed in real-time. Each $P - \omega$ pair in Figure 6 corresponds to a tidal current speed, which shows a non-linearity behavior with the explicit function $v = f(P, \omega)$. The ANN with several hidden layers of neurons learns this correlation after training and predicts the tidal current speed used in the MLCT controller.

Multiple neurons in a hidden layer of an ANN with a vector input are shown in Figure 7, where $p_1, p_2, \ldots, p_R$ are elements of the input vector $\mathbf{P}$, and the weight vector is $\mathbf{W}$.

Output $\mathbf{a}$ is obtained by

$$\mathbf{a} = \mathbf{f}(\mathbf{Wp} + \mathbf{b}), \tag{9}$$

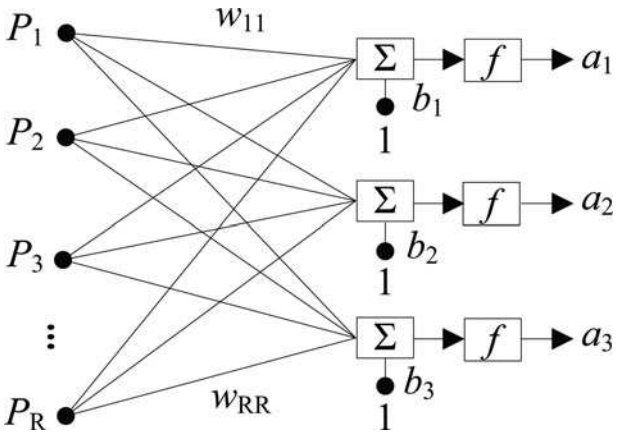

FIGURE 7. Multiple neurons in one hidden layer.

$$\mathbf{a} = \begin{bmatrix} a_1 \\ a_2 \\ \vdots \\ a_R \end{bmatrix}, \mathbf{b} = \begin{bmatrix} b_1 \\ b_2 \\ \vdots \\ b_R \end{bmatrix}, \tag{10}$$

$$\mathbf{W} = \begin{bmatrix} w_{11} & w_{12} & \cdots & w_{1R} \\ w_{21} & w_{22} & \cdots & w_{2R} \\ \vdots & \vdots & \ddots & \vdots \\ w_{R1} & w_{R2} & \cdots & w_{RR} \end{bmatrix}, \tag{11}$$

where **b**, a scalar bias, and **W** are adjustable so that the neural network is trained accordingly. These parameters are trained using a back-propagation method or extreme learning machine for fast-speed applications. f represents the transfer function used in the layers for different purposes. Multiple hidden layers are often adopted for better prediction accuracy [17].

In this article, the data generated from each characteristic curve in Figure 6 to are train a feedforward neural network, which is then used to estimate tidal current speed. In Figure 8, the first stage (speed estimation) uses one hidden layer of 60 neurons, and the second stage uses one hidden layer of 5 neurons to generate the reference rotating speed. The data used in training the ANN can be found in Table B.1 in Appendix

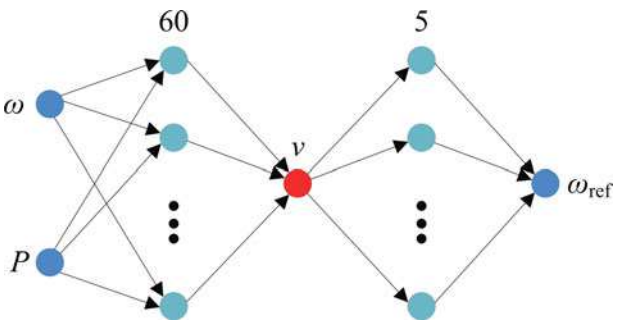

FIGURE 8. Feedforward neural network.

λ	ω	P
0.9	4.5	436.5
1.8	9.0	1487
2.7	13.5	2291
3.6	18.0	2561
4.5	22.5	2369
5.4	27.0	1881
6.3	31.5	1075

TABLE 1. Data for speed estimation stage

B. In the table, the first column is the tidal current speed, which serves as the input of the ANN. The second and third columns are the outputs for the MPPT control and the MLCT control. It can be seen from the data that when the tidal current speed is under 2.2 m/s, the inputs of the two neural networks are the same. When it exceeds this speed, the rotating speed under MLCT control becomes higher. Table 1 shows the speed estimation samples.

Training the neural networks is done with the MATLAB function "fignet". One can also use (The MathWorks, Natick, Massachusett, USA) "gensim" to convert the neural network function to a Simulink block. This enables the neural networks to be embedded into the real-time simulation environment.

3.2. Back-to-back Converter Implementation

Both MLCT and MPPT have been implemented via a back-to-back power electronic converter system. Since the output power of the tidal turbine fluctuates and the frequency and the magnitude of the terminal voltage varies, back-to-back converters are employed to interface the tidal generator system with the power grid because of its flexible control [18]. It consists of a machine-side converter and a grid-side converter, which connects to the grid through a filter. Between the two converters is the DC link, which absorbs the instantaneous active power difference and works as a voltage source for the converters. The grid-side converter, maintains a constant DC-link voltage and controls the active power and the reactive power delivered to the grid. The machine-side converter controls power generation, which is able to apply different control strategies. Control algorithms for the two converters are decoupled and operate at different AC frequencies. The control block diagram of the machine-side converter is shown in Figure 9. Here i_{ds-ref} is the control reference of the d axis current, and $i_{ds-ref} = 0$; i_{qs-ref} is the control reference of the q-axis current, which plays an important role in extracting the maximum power from the tides. Zero d-axis current control is applied to ensure a linear relation between electromagnetic torque and q-axis current for both salient and non-salient rotor

Downloaded by [University of Connecticut] at 13:38 11 January 2018

Downloaded by [University of Connecticut] at 13:38 11 January 2018

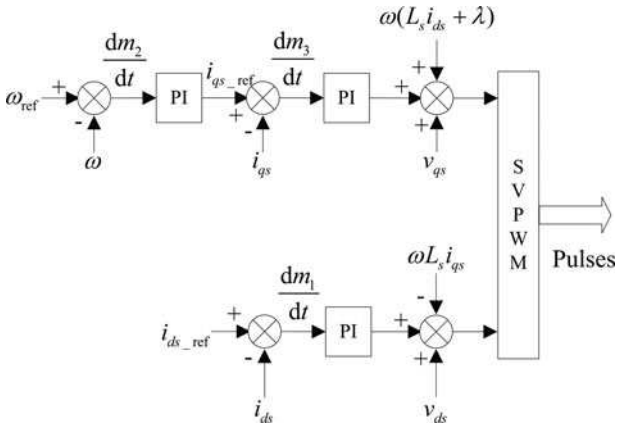

FIGURE 9. Control diagram of the machine-side converter.

PMSG [19]. Subsequently, the grid-side converter controller, as shown in Figure 10, is controlled to output constant active power to the grid and keep the DC-link voltage constant. The q-axis reference current is set to zero to eliminate reactive power, and all of the grid voltage is in the d-axis.

4. CASE STUDY

In this section, extensive numerical tests have been conducted to validate the effectiveness of MLCT. In case 1, tidal current speed data are used to test the system performance under normal conditions. The purpose is to show how MLCT reduces the mechanical torque and electromagnetic torque in the tidal system and how it compares to MPPT. In case 2, neural network and sensor speed are used to generate the reference rotating speed of the turbine to show how a neural network improves reliability of the tidal generation system. Finally, case 3 describes the use of a filter at the machine side of the control system to help reduce the torque ripples, which increases the life cycle of the tidal turbine shaft.

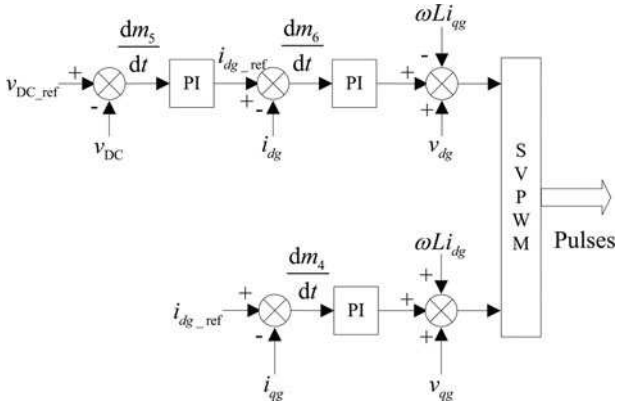

FIGURE 10. Control diagram of the grid-side converter.

A 12-hr simulation is carried- out with massive real tidal current speed data as input. Models with this much detailed and big data can hardly be simulated in conventional PC-based power system simulators, such as PSCAD or SimPowerSystems. Hence, to enable fast simulations, Opal-RT real-time the hardware-in-the-loop simulator is employed (Opal-RT Technologies, Montréal, Québec, Canada). With multi-core processors and large memory, the Opal-RT is able to run simulations in real-time and store large amounts of data [20]. A schematic of the model as implemented in the Opal-RT environment is shown in Figure 11.

4.1. Case I: Normal Condition with Real Tidal Current Data

The MPPT and MLCT performance are compared. Simulation results in Figure 12 show that at low tidal current speeds, both strategies capture the maximum power available. However, when the tidal current increases, MPPT captures the most power at the expense of high mechanical torque T_m and electromagnetic torque T_e. MLCT, however, greatly reduces the torque as shown in the subplots (a) and (b), with a small difference in captured power compared to MPPT, shown in subplot (c). Subsequently, the mechanical stress in the shaft is reduced, which leads to significant life extension and overall cost reduction through MLCT. Table 2 shows results based on Eq (2) and the Miner's rule in Eq. (3). The MLCT strategy has 2.82% expected life expenditure of MPPT control, which means the life cycle of the tidal turbine blades will be extended to 35 times. Similarly, the life cycle of the shaft will be extended to 38.8 times with captured power a little less than MPPT during the life cycle of the tidal system with MPPT. Intuitively, because the life cycle is about 35 times longer, MLCT has the potential to harvest more energy than that from MPPT.

4.2. Case II: The Effect of Using ANN-based Sensor-less Design and That of Speed Sensor

This case study compares the effect of using an ANN technique sensorless design and that of a speed sensor in estimating the tidal current speed. The simulation results are presented in

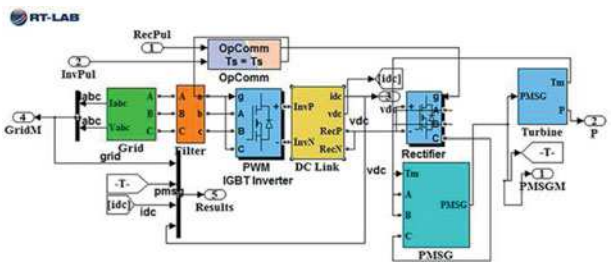

FIGURE 11. RT-lab model

Downloaded by [University of Connecticut] at 13:38 11 January 2018

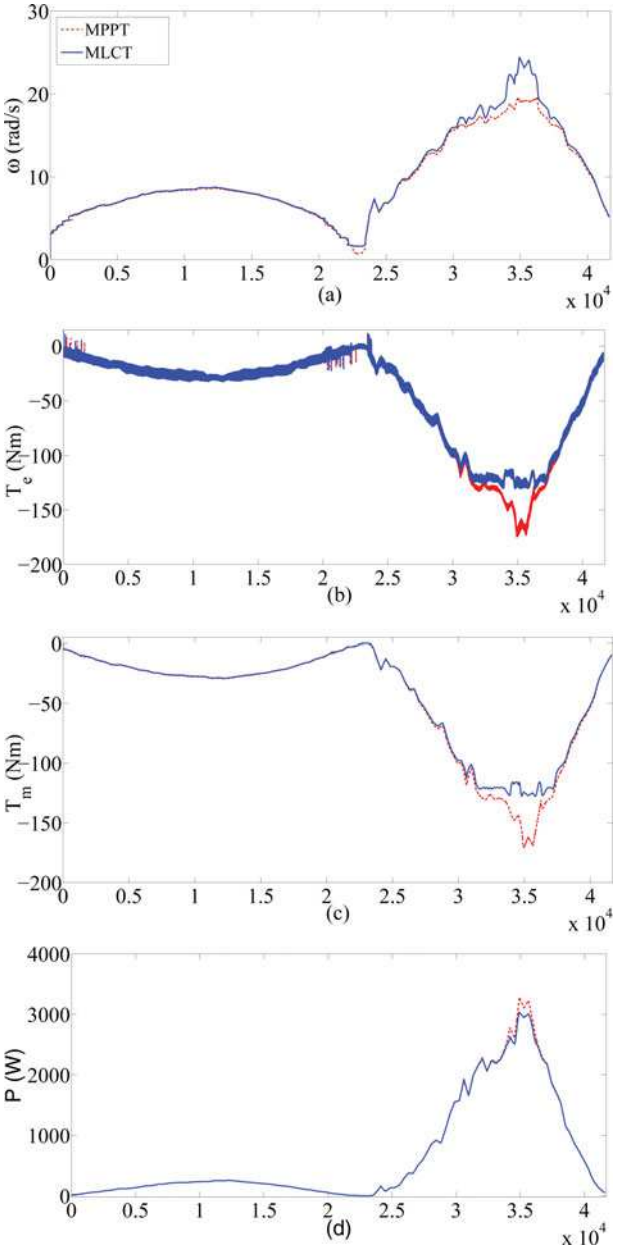

FIGURE 12. Simulation results for Case I.

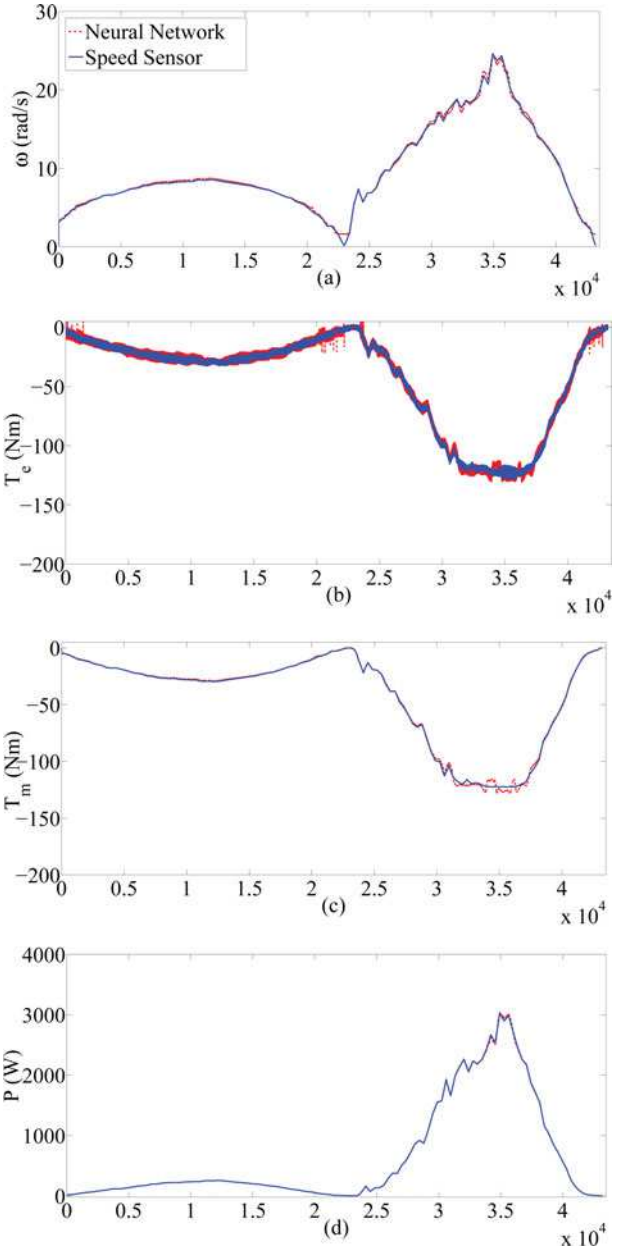

FIGURE 13. Simulation results for Case II.

	T_m		T_e		Energy
	Max (Nm)	D	Max (Nm)	D	(kWh)
MPPT	171.14	4.07×10^{-4}	188.54	1.2×10^{-3}	7.724
MLCT	127.96	1.15×10^{-5}	146.37	3.21×10^{-5}	7.606
%	74.77%	2.82%	77.63%	2.58%	98.47%

TABLE 2. Results for Case I

Figure 13, and the quantitative comparisons in Table 3 show that the ANN and the speed sensor produce similar results. Although the result with the speed sensor is smoother, this might be due to several reasons, such as the model does not take into account the noise and delay in the sensor in real-time conditions, and/or the ANN needs to be trained further. However, the simulation results confirm the use of ANNs to estimate the tidal current speed. The advantages of using an ANN over sensor speed are as follows: (i) tidal current speed estimation is made directly by the ANN, (ii) the ANN only requires simple measurements of the captured power and rotating

	T_m		T_e		Energy
	Max	D	Max	D	(kWh)
NN	127.7	2.3×10^{-7}	131.0	2.3×10^{-6}	7.6
Sensor	122.8	1.1×10^{-7}	128.3	1.6×10^{-6}	7.6
Sensor/NN	96.2%	49.6%	97.9%	70.4%	99.95%

TABLE 3. Results for Case II

speed of the rotor to estimate the tidal current speed, and thus (iii) the ANN reduces the cost of installing and maintaining underwater sensors and significantly improves the reliability of the system.

4.3. Case III: Simulations Comparing the Electromagnetic Torque with and Without Filter

Normally it is desirable for a tidal turbine generator to produce a ripple-free electromagnetic torque, because ripples lead to speed oscillations, causing vibrations in the shaft. These vibrations add shear stress, which could result in deterioration in the performance of the shaft and may reduce the life cycle of the turbine. To reduce the torque ripples, a low-pass filter was added at the input of the q-axis current in the machine control side, since the q-axis current directly tracks the electromagnetic torque. Also, the space vector pulse-Width modulator (SVPWM), which subdivides the switching period into several states helps to synthesize the voltage vectors to generate minimum torque ripples. The torque ripple is defined as

$$\text{Torque ripple} = \frac{T_{\max} - T_{\min}}{T_{\text{avg}}} \times 100, \tag{12}$$

where $T_{\max}$ is the maximum torque ripple, $T_{\min}$ is the minimum torque ripple, and T_{avg} is the average torque ripple. In the simulation results shown in Figure 14(a), the torque ripples in the system increases to around 40% without a low-pass filter. But adding a low-pass filter reduces the ripples to about 10%, as shown in Figure 14(b), thereby increasing the lifespan of the turbine.

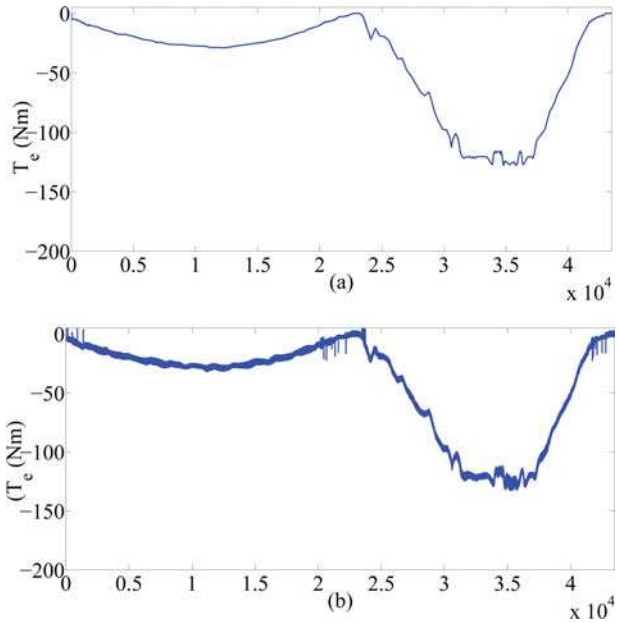

FIGURE 14. Simulation results for Case III:(a) with filter and (b) without filter.

5. CONCLUSION

High tidal current has significant influences on a tidal generation system. The torque analysis shows that the mechanical torque and the electromagnetic torque fluctuation could cause severe damage to the turbine blades and shaft, thereby reducing the lifespan of the system. In this article, MLCT is introduced, developed, and tested in a real-time simulation environment to increase the life cycle of a tidal generation system. The effectiveness of MLCT is confirmed by comparing it to MPPT. MLCT applies the MPP control to the system when the tidal speed range is low and a constant torque control when the tidal speed range is high. Simulation results show MLCT greatly reduces the stress on tidal turbine shafts and extends the life by more than 30 times at a little cost of power under the test scenarios.

FUNDING

The first author would like to thank the National Science Foundation GK-12 Program for research support under Award Number 0947869. The authors would also like to thank the National Science Foundation for research support under grant CNS-1419076.

REFERENCES

[1] Rowell, M. "Experimental evaluation of mixer ejector hydrokinetc turbine (MEHT) at two tidal energy test sites and in a tow tank," 2013, available at: *http://www.mrec.umassd.edu/media/supportingfiles/mrec/ agendasandpresentations/ 4thconference/matthew_rowell.pdf*

[2] Shahsavarifard, M. "Effect of shroud on performance of horizontal axis hydrokinetic turbine," 2013, available at: *http://www.mrec.umassd.edu/ 4thconference*

[3] Zhao Y., and Su X., "Tidal energy: Technologies and recent developments, *2010 IEEE International Energy Conference and Exhibition (EnergyCon)*, pp. 618–623, Manama, Bahrain, 18–22 December 2010.

[4] Huai, W., Liserre, M., Blaabjerg, F., De Place Rimmen, P., Jacobsen, J. B., Kvisgaard, T., and Landkildehus, J., "Transitioning to physics-of-failure as a reliability driver in power electronics,"

Downloaded by [University of Connecticut] at 13:38 11 January 2018

Downloaded by [University of Connecticut] at 13:38 11 January 2018

IEEE J. Emerging Selected Topics Power Electron., Vol. 2, No. 1, pp. 97–114, 2014.

[5] Benelghali, S., El Hachemi Benbouzid, M., Charpentier, J. F., Ahmed-Ali, T., and Munteanu, I. "Experimental Validation of a marine current turbine simulator: Application to a permanent magnet synchronous generator-based system second-order sliding mode control," *IEEE Trans. Ind. Electron.*, Vol. 58, No. 1, pp. 118–126, 2011.

[6] Sean, K., "Failed tidal turbine explained at symposium," available at: *http://www.cbc.ca/news/canada/nova- scotia/failed-tidal-turbine-explained- at-symposium-1.1075510*

[7] Walker, D. N., Adams, S. L. and Placek, R. J., "Torsional vibration and fatigue of turbine-generator shafts," *IEEE Trans. Power Apparatus Sys.*, Vol. 100, No. 11, pp. 4373–4380, 1981.

[8] Jackson, M. C., Umans, S. D., Dunlop, R. D., Horowitz, S. H., and Parikh, A. C., "Turbine-generator shaft torques and fatigue: Part I – simulation methods and fatigue analysis," *IEEE Trans. Power Apparatus Syst.*, Vol. 98, No. 6, pp. 2299–2307, 1979.

[9] Hammons, T. J. "Accumulative fatigue life expenditure of turbine/generator shafts following worst-case system disturbances," *IEEE Trans. Power Apparatus Syst.*, Vol. 101, No. 7, pp. 2364–2374, 1982.

[10] Song-Manguelle, J., Schroder, S., Geyer, T., Ekemb, G., and Nyobe-Yome, J. M., "Prediction of mechanical shaft failures due to pulsating torques of variable-frequency drives," *IEEE Trans. Industry App.*, Vol. 46, No. 5, pp. 1979–1988, 2010.

[11] Iliev, C. and Val, V., "Tidal current turbine reliability: power take-off train models and evaluation," 3rd *International Conference on Ocean Energy*, Bilbao, 6 October 2010.

[12] Adhikari, S., and Fangxing, L., "Coordinated V-f and P-Q control of solar photovoltaic generators with MPPT and battery storage in microgrids," *IEEE Trans. Smart Grid*, Vol. 5, No. 3, pp. 1270–1281, 2014.

[13] Pucci, M., and Cirrincione, M., "Neural MPPT control of wind generators with induction machines without speed sensors," *IEEE Trans. Ind. Electron.*, Vol. 58, No. 1, pp. 37–47, 2010.

[14] Ariduru, S., *Fatigue Life Calculation by Rainflow Cycle Counting Method*, MSME Thesis, Middle East Technical University, Ankara, Turkey, 2004.

[15] Mullane, A., Bryans, G. and O'Malley, M., "Kinetic energy and frequency response comparison for renewable generation systems," *2005 International Conference on Future Power Systems*, p. 6, Amsterdam, 18 November 2005.

[16] Ben Elghali, S. E., Balme, R., Le Saux, K., Benbouzid, M. E. H., Charpentier, J. F., and Hauville, F., "A simulation model for the evaluation of the electrical power potential harnessed by a marine current turbine," *IEEE J. Oceanic Eng.*, Vol. 32, No. 4, pp. 786–797, 2008.

[17] Beale, M. H., Hagan, M. T., and Demuth, H. B., " Neural network toolbox user's guide," 2014, availabel at: *http://www.mathworks.com/help/pdf_doc/ nnet/nnet_ug.pdf*

[18] Bifaretti, S., Zanchetta, P., Iov, F., and Clare, J. C., " 13th Predictive current control of a 7-level AC-DC back-to-back converter for universal and flexible power management system," *Power Electronics and Motion Control Conference* (EPE-PEMC 2008), pp. 561–568, Poznan, 1–3 September 2008.

[19] Kan L., and Zhu, Z. Q., "Online estimation of the rotor flux linkage and voltage-source inverter nonlinearity in permanent magnet synchronous machine drives," *IEEE Trans. Power Electronics*, Vol. 29, No. 1, pp. 418–427, 2014.

[20] Belanger, J., Venne, P., and Paquin, J., "The what, where and why of real-time simulation," *IEEE PES General Meeting*, pp. 37–49, Minneapolis, 25–29 July 2010.

APPENDIX

A. MODEL OF THE TIDAL SYSTEM

The turbine model is

$$P = 0.5\rho\pi R^2 v^3 C_p(\lambda), \tag{A.1}$$

$$C_p(\lambda) = c_5\lambda^5 + c_4\lambda^4 + c_3\lambda^3 + c_2\lambda^2 + c_1\lambda + c_0, \tag{A.2}$$

where c_0 to c_5 are constants, ρ is the water density, and C_p is the tidal turbine power coefficient. λ is the tip speed ratio, which is defined by

$$\lambda = \frac{\omega R}{v}. \tag{A.3}$$

The model of the PMSG is

$$v_{ds} = R_s i_{ds} + L_d \frac{di_{ds}}{dt} - p\omega L_q i_{qs}, \tag{A.4}$$

$$v_{qs} = R_s i_{qs} + L_q \frac{di_{qs}}{dt} + p\omega L_d i_{ds}, \tag{A.5}$$

$$P_e = \frac{3}{2}(v_{ds} i_{ds} + v_{qs} i_q s), \tag{A.6}$$

$$T_e = \frac{3}{2} p\psi_m i_{qs}, \tag{A.7}$$

$$\tag{A.8}$$

where v_{ds} and v_{qs} are the q-axis and d-axis stator terminal voltage, respectively; i_{ds} and i_{qs} are the q-axis or d-axis stator currents, respectively; L_q and L_d are the q-axis or d-axis inductances of the PMSG, respectively; R_s is the resistance of the stator windings; ω is the electrical angular velocity of the rotor; and p is the number of pole pairs of the PMSG.

The model of drive train is

$$J\frac{d\omega}{dt} = T_m - T_e, \tag{A.9}$$

$$T_m = \frac{P}{\omega}. \tag{A.10}$$

$$\tag{A.11}$$

The model of machine side converter with controller is

$$i_{ds}^* = 0, \tag{A.12}$$

$$\frac{dm_1}{dt} = i_{ds}^* - i_{ds}, \tag{A.13}$$

$$v_{ds}^* = k_{P1}(i_{ds}^* - i_{ds}) + k_{I1} m_1 - p\omega L_s i_{qs} + R_s i_{ds}, \tag{A.14}$$

$$\frac{dm_2}{dt} = \omega^* - \omega, \tag{A.15}$$

$$\omega^* = g(v), \tag{A.16}$$

$$i_{qs}^* = k_{P2}(\omega^* - \omega) + k_{I2} m_2, \tag{A.17}$$

$$\frac{dm_3}{dt} = i_{qs}^* - i_{qs}, \tag{A.18}$$

$$v_{qs}^* = k_{P3}(i_{qs}^* - i_{qs}) + k_{I3}m_3 + R_s i_{qs} + p\omega L_s i_{ds} + p\omega\psi_m, \quad (A.19)$$

where k_P and k_I are the proportional and integral gains of the PI controller; ψ_m is the flux linkage generated by the permanent magnet.

The model of the filter is

$$u_{qg} = v_{qg} + L_g\frac{di_{qg}}{dt} + \omega_g L_g i_{dg}. \quad (A.20)$$

$$u_{dg} = v_{dg} + L_g\frac{di_{dg}}{dt} - \omega_g L_g i_{qg}, \quad (A.21)$$

(A.22)

The model of the grid-side converter with controller is

$$i_{qg}^* = 0, \quad (A.23)$$

$$\frac{dm_4}{dt} = i_{qg}^* - i_{qg}, \quad (A.24)$$

$$u_{qg}^* = k_{P4}(i_{qg}^* - i_{qg}) + k_{I4}m_4 + \omega L_g i_{dg} + v_{qg}, \quad (A.25)$$

$$\frac{dm_5}{dt} = v_{DC}^* - v_{DC}, \quad (A.26)$$

$$i_{qg}^* = k_{P5}(v_{DC}^* - v_{DC}) + k_{I5}m_5, \quad (A.27)$$

$$\frac{dm_6}{dt} = i_{dg}^* - i_{dg}, \quad (A.28)$$

$$u_{dg}^* = k_{P6}(i_{dg}^* - i_{dg}) + k_{I6}m_6 - \omega L_g i_{qg} + v_{dg}, \quad (A.29)$$

(A.30)

The model of DC link is

$$C\frac{dv_{DC}}{dt} = \frac{P_t}{v_{DC}} - \frac{P_g}{v_{DC}}. \quad (A.31)$$

APPENDIX B. SYSTEM DATA

Tidal current speed (m/s)	MPPT rotor speed (rad/s)	MLCT rotor speed (rad/s)
0.1	0.72	0.72
0.2	1.44	1.44
0.3	2.16	2.16
0.4	2.88	2.88
0.5	3.60	3.60
0.6	4.32	4.32
0.7	5.04	5.04
0.8	5.76	5.76
0.9	6.48	6.48
1.0	7.20	7.20
1.1	7.92	7.92
1.2	8,64	8,64
1.3	9.36	9.36
1.4	10.08	10.08
1.5	10.80	10.80
1.6	11.52	11.52
1.7	12.24	12.24
1.8	12.96	12.96
1.9	13.68	13.68
2.0	14.40	14.40
2.1	15.12	15.12
2.2	15.84	15.84
2.3	16.56	16.62
2.4	17.28	18.72
2.5	18.00	20.73
2.6	18.72	22.69
2.7	19.44	24.62
2.8	20.16	26.52
2.9	20.88	28.41
3.0	21.60	30.28

(Continued)

TABLE B1. Data for reference generation stage

BIOGRAPHIES

Taofeek Orekan received his B.Sc. in electrical engineering from Southern Polytechnic State University. He is currently pursuing his Ph.D. in electrical engineering at University of Connecticut, Storrs. His research interests include ocean power systems and smart grid.

Zhibing Zhao received his B.Sc. from Tsinghua University, China, and his M.Sc. from University of Connecticut, Storrs, both in electrical engineering. His research interest is in renewable energy.

Peng Zhang received his Ph.D. in electrical engineering from University of British Columbia, Vancouver, BC, Canada. He is an assistant professor of electrical engineering at the University of Connecticut, Storrs. He was a system planning engineer at British Columbia Hydro and Power Authority (2006–2010), where he planned and designed seven large wind farms. His recent efforts have led to the creation of UCONN's Depot Campus Microgrid and UCONN's first photovoltaic array, a study for hardening northeast utilities power infrastructure against extreme weathers, and the Building Innovator Award from U.S. DOE. His research interests include grid integration of renewable energy systems, power system resilience, smart grids, microgrids, and smart ocean technologies. He is a registered professional engineer in British Columbia, Canada, and an editor of *Electric Power Components and Systems*.

Jian Zhang received his B.Sc. in electrical engineering from Northeast Dianli University, Jilin, China, in 2009 and his Ph.D. in electrical engineering from North China Electric Power University, Beijing, China, in 2014. He was a visiting scholar at

Downloaded by [University of Connecticut] at 13:38 11 January 2018

University of Connecticut, Storrs, from November 2013 to November 2014. His research interests include power system stability, subsynchronous oscillation, power electronics applications to renewable energy systems, and microgrid control.

Shengli Zhou received his B.S. in 1995 and his M.Sc. in 1998 from University of Science and Technology of China, Hefei, both in electrical engineering and information science. He received his Ph.D. in electrical engineering from University of Minnesota, Minneapolis, in 2002. He is now a full professor with the Department of Electrical and Computer Engineering at the University of Connecticut, Storrs. He is now an associate editor for *IEEE Journal of Oceanic Engineering*. He received the 2007 ONR Young Investigator award and the 2007 Presidential Early Career Award for Scientists and Engineers (PECASE). He was elected to be an IEEE Fellow in 2014. His general research interests lie in the areas of wireless communications and signal processing. His recent focus is on underwater acoustic communications and networked systems.

Jun-Hong Cui received he B.Sc. in computer science from Jilin University, China, in 1995, her M.Sc. in computer engineering from Chinese Academy of Sciences in 1998, and her Ph.D. in computer science from UCLA in 2003. Currently, she is on the faculty of the Computer Science and Engineering Department at University of Connecticut. Her research interests cover the design, modeling, and performance evaluation of networks and distributed systems. Her recent research mainly focuses on exploiting the spatial properties in the modeling of network topology, network mobility, group membership, scalable and efficient communication support in overlay and peer-to-peer networks, and algorithm and protocol design in underwater sensor networks.

S. Zhou and J.-H. Cui have an ownership interest in AquaSeNT, which is a marine sensor and communication technology firm that develops underwater wireless communication technology.

Downloaded by [University of Connecticut] at 13:38 11 January 2018